Manuscript
Click here to access/download;Manuscript;Rood_et_al_SRL_final_resubmis

San Andreas fault earthquake hazard model validation using probabilistic analysis of precariously balanced rocks and Bayesian updating

Anna H. Rood[1,2*], Peter J. Stafford[1], Dylan H. Rood[3]

[1]Department of Civil and Environmental Engineering, Imperial College London, London, SW7 2AZ, UK.

[2]Global Earthquake Model (GEM) Foundation, 27100 Pavia, Italy.

[3]Department of Earth Science and Engineering, Imperial College London, London, SW7 2AZ, UK.

**Corresponding author: anna.rood@imperial.ac.uk*

ABSTRACT

The Mojave section of the San Andreas fault is the closest section to the megacity of greater Los Angeles. A major issue is that the life-threatening hazard estimate to the population of a future rare, large earthquake on this fault section is highly uncertain and untested at timescales and ground motions beyond limited historical recordings. Of relevance to this issue is that despite the past tens of thousands of years of San Andreas fault earthquakes, the nearby precariously balanced rocks at Lovejoy Buttes have survived these ground motions. Therefore, the fragility and age of these precariously balanced rocks provide crucial ground-motion constraints over the timescales of rare, large San Andreas fault earthquakes. We rigorously validate and update an earthquake hazard model for the Mojave section of the San Andreas fault using the independent observational data of precariously balanced rock survival at Lovejoy Buttes. The joint probability of survival of all five studied precariously balanced rocks was used to validate the hazard estimates and reweight the estimates using new Bayesian updating methods to deliver an improved, precariously balanced rock-informed earthquake hazard estimate. At an annual frequency of exceedance of $1x10^{-4}$ yr^{-1}, equivalent a mean return period of 10,000 years, the precariously balanced rock survival data significantly reduced mean hazard ground-motion estimate by 65% and the 5^{th}-95^{th} fractile uncertainty range by 72%. The magnitude of this inconsistency provides striking evidence for the need to reevaluate both the source and ground motion components of our earthquake hazard model for the southern San Andreas fault.

INTRODUCTION

The San Andreas fault is one of the most seismically active faults in the United States (U.S.), which presents a significant hazard to human life, societal infrastructure, and the environment in southern California. The extensive study and characterization of the San Andreas fault has revealed not only the complexity of this plate boundary fault system but also the limitations of scientists' understanding of earthquake processes. These difficulties generate substantial uncertainty in the estimation of the ground-motion intensity and potential destruction of future earthquakes. Probabilistic seismic hazard analysis (PSHA) is the ubiquitous framework used not only in California but globally to develop earthquake hazard estimates for use in land use planning, building-code development, disaster preparation and emergency response, and the siting, design, and maintenance of critical facilities. It is established that a state-of-the-art PSHA model should include validation of the earthquake hazard results with independent observations (Gerstenberger *et al.*, 2020). However, for rare, large earthquakes beyond the timescales of recorded historical earthquakes it is necessary to exploit geologic data for such validation.

The survival of precariously balanced rocks (PBRs) in proximity to seismically active faults provides valuable independent observations about the upper bound on past ground motions that occurred at a site, which can be used to validate PSHA hazard estimates for the site (Anderson *et al.*, 2011; Brune, 1996; Stirling *et al.*, 2020). The fragility and age of such independent PBR data have previously been used to validate site-specific PSHA models for sites of critical infrastructure (Hanks *et al.*, 2013; Rood *et al.*, 2020; Stirling *et al.*, 2021). However, for PBRs to become a common-practice PSHA validation tool, site-specific PSHA models need to be readily constructed for the site of the PBRs. Importantly, this site-specific PBR validation should consider the uncertainty in the characterization of the PBRs and test the entire distribution of hazard estimates.

The use of Bayesian techniques of updating prior information in PSHA models with independent observational information offers the opportunity to incorporate these independent PBR observations to update and improve hazard estimates of future earthquakes. Specifically, Bayesian techniques provide an objective method for attributing weights to the branches of a PSHA model logic tree. Previously, such Bayesian logic tree weight re-weighting methods using PBR data were proposed by Rood *et al.* (2020), however, these methods have never been implemented, until now.

In this present study, we construct a site-specific PSHA model, using the UCERF3 and SWUS models (see Methods) for an important PBR site in southern California near the Mojave South section of the San Andreas fault, the Lovejoy Buttes site. We validate the ground-motion estimates for the site using the fragility and age data of the PBRs. Specifically, we assess the probability of

survival of the PBRs at Lovejoy Buttes for each of the alternative logic tree end-branch ground-motion estimates output from our PSHA model. Finally, we then use this probability of survival data to conduct a Bayesian updating of the logic tree end-branch weights to improve the ground-motion estimates. The Mojave South section is the closest part of the San Andreas fault to the population and infrastructure of Los Angeles, therefore, our validation of earthquake hazard for Lovejoy Buttes potentially has important implications for the earthquake hazard for Los Angeles.

PSHA Background

PSHA is the regulatory required framework to estimate the expected rate of exceedance of a particular ground-motion level at a particular site (SSHAC, 1997; SSHAC, 2012). The first necessary component of a PSHA model is a seismic-source characterization (SSC) model. A SSC model estimates the rate of occurrence of all possible ruptures on all local active faults. The second necessary component of a PSHA model is a ground-motion characterization (GMC) model. A GMC model is composed of a suite of semi-empirical ground-motion models (GMMs) that estimate the level of ground shaking given magnitude, distance, and other predictor variables. These two components are then combined to calculate the expected rates of exceedance for different ground-motion levels, which is called a hazard curve (Baker *et al.*, 2021). To accommodate the epistemic uncertainties between alternative models and parameters within the SSC model and GMC model, a logic tree framework is employed, in which different models or parameters occupy different branches of the tree (Kulkarni *et al.*, 1984). Weights are assigned to each branch, and the weighted calculations lead to a distribution of hazard curves (Atkinson *et al.*, 2014).

The other key uncertainty parameter modelled in PSHA is the random (aleatory) variability of the GMMs about the median prediction, which controls the shape of the hazard curves (Bommer & Abrahamson, 2006). This variability is typically handled using the ergodic assumption, where the variability in ground motion at a single source-path-site combination is treated the same as the variability in ground motion observed in global databases. Therefore, these ergodic GMMs use average source, path, and site effects derived from global databases of ground-motion recordings (Anderson & Brune, 1999b). This ergodic assumption is typically necessary due to the sparse recording of ground-motion data to constrain source-, path-, and site-specific effects.

The variance of the GMM distribution can be separated into many different components; not just between-event and within-event (Atik *et al.*, 2010). In particular, the use of single-station sigma has become standard practice in partially or fully site-specific PSHA studies (Atkinson, 2006; Rodriguez- Marek *et al.*, 2014). The single-station approach is straightforward to implement in PSHA because, first, the median hazard is computed for a reference rock site condition with an

ergodic GMM and the ergodic sigma, i.e., standard deviation, is reduced. Then, second, the site-specific effect adjustment to the median and its epistemic uncertainty are computed using traditional site-response methods (Rodriguez- Marek et al., 2014). This partially nonergodic GMM reduces aleatory variability whereas epistemic uncertainty often increases due to the uncertainty in characterizing these repeatable effects.

The Lovejoy Buttes Site

Lovejoy Buttes is a steep, isolated, rocky hill to the west of the city of Lake Los Angeles in north-eastern Los Angeles County (Figure 1). The Lovejoy Buttes site is ~15 km from the closest point on the Mojave South section of the San Andreas fault, which is the single dominant seismic source at the site. This section of the San Andreas fault is believed to have been ruptured by the estimated M7.3 Wrightwood earthquake in 1812 (Toppozada *et al.*, 2002) and 44 years later by the estimated M7.7–M7.9 Fort Tejon earthquake (Sieh *et al.*, 1989; Zielke *et al.*, 2012). Damage caused by these two earthquakes was recorded at the nearby San Gabriel mission (Grant Ludwig *et al.*, 2015; Toppozada *et al.*, 2002). Historical records on this section of the San Andreas fault are only considered to be complete since ~1800 A.D (Toppozada *et al.*, 2002), therefore, the complete history of the earthquake cycle over thousands of years has not been recorded. However, the paleoseismic sites nearby to Lovejoy Buttes, Pallett Creek and Wrightwood, provide the longest records for the San Andreas fault. These two sites both have over 10 paleoearthquake ages determined from radiocarbon dating of faulted sediments (Biasi *et al.*, 2002; Fumal *et al.*, 2002; Scharer *et al.*, 2007; Sieh *et al.*, 1989). This historic and prehistoric record of large earthquake events imparts a significant hazard of large earthquakes in the future near both Lovejoy Buttes and the city of Los Angeles.

Lovejoy Buttes is composed of Cretaceous granitic quartz monzonite rock and is surrounded by low-relief Holocene alluvial gravel, sand, and silt (Dibblee & Minch, 2008). At Lovejoy Buttes, PBRs have formed as granitic corestones, which initially developed in the subsurface by weathering along bedrock joints and fractures during a period of low erosion (Oberlander, 1972). These subsurface corestones were then exhumed by the stripping of surrounding regolith and saprolite as the erosion rate increased in response to uplift as stresses transferred onto the modern trace of the San Andreas fault. Since exhumation negligible erosion of the PBR has occurred, therefore, the PBRs have been preserved in their current fragile geometry balanced on the rock outcrops since they were exhumed (Hall *et al.*, 2019).

The distribution of PBR fragilities at Lovejoy Buttes has been shown to be depleted in the most fragile PBRs, relative to a low seismicity PBR site and also with distance from the San Andreas

fault (Anderson *et al.*, 2011; Brune, 1999). An interpretation of this result is that the most fragile PBRs at Lovejoy Buttes were toppled during previous earthquakes, whereas the more stable PBRs survived. Anooshehpoor *et al.* (2004) investigated the variation of toppling of wooden blocks for synthetic seismograms generated for an Mw 8.0 San Andreas earthquake event at Lovejoy Buttes. The numerical results provide a peak ground acceleration (PGA) constraint of about 0.5g (±0.1 g) at Lovejoy Buttes. Previous studies of these PBRs have shown that the survival of the PBRs at Lovejoy Buttes is inconsistent with the hazard estimates for the site (Anderson *et al.*, 2014; Purvance *et al.*, 2008b).

Importantly, both Abbott (2001) and Stirling *et al.* (2002) showed that slightly amplified recorded PGAs at Lovejoy Buttes means that site conditions do not appear to explain the preservation of the precarious rocks. Rood *et al.* (*2022*) characterized both the fragility (probability of a PBR toppling given an intensity of ground motion) and fragility age (the time when the PBR-pedestal contact became exhumed by erosion of the surrounding regolith and, therefore, became free to potentially topple due to earthquake ground shaking) of five PBRs at the Lovejoy Buttes site (Figure 1c). The age of these five PBRs ranges from ~10 to ~50 ka, which provides the desired ground-motion constraints over the timescale of rare, large earthquakes on the San Andreas fault.

The wealth of previous research and PBR data at Lovejoy Buttes was a key motivator in its selection as the case study to apply the new Rood *et al.* (*2022*) PBR fragility and fragility age data to further advance PBR research. We will apply the latest PBR validation methods to validate some of the latest PSHA component SSC and GMC models. We calculate the probability of survival of the PBRs at Lovejoy Buttes to individually validate each of the alternative PSHA model hazard estimates for the site. Of great significance, is that we then develop a procedure to consider all the uncertainties in the PBR characterization to update the logic tree end-branch weights using Bayesian updating. The improved, PBR-informed hazard estimates for the site directly place constraints on our PSHA model estimates for the Mojave South section of the San Andreas fault.

METHODS

A PSHA model was constructed for the Lovejoy Buttes site for the purpose of implementing advancements in the PBR methodology to validate the PSHA hazard estimates with the independent PBR data. Our Lovejoy Buttes PSHA model was similarly constructed using some of the latest advances in both the SSC model (UCERF3) and GMC model (SWUS) components of PSHA. The PSHA model developed in this study is not intended as a standardized PSHA method for PBR sites. In future studies, the geographic location and seismotectonic setting of the study site as well as the requirements of the study should guide the PSHA model developed for PBR sites.

Lovejoy Buttes Seismic Source Characterization

The Lovejoy Buttes site is as straight-forward a location as possible for assembling our SSC model as there is both a single dominant fault and a simple source-to-site geometry. The advantage of these factors is that there is a constant distance from the closest point on the San Andreas Mojave South section to the Lovejoy Buttes site for all possible ruptures on the fault section. The Third Uniform California Earthquake Rupture Forecast (UCERF3), developed by the U.S. Geological Survey and the Working Group on California Earthquake Probabilities, provides estimates of the magnitude, location, and time-averaged frequency of potentially damaging earthquakes in California (Field *et al.*, 2013). In the UCERF3 model, the Mojave South section of San Andreas fault is divided into 15 subsection each ~7 km long. UCERF3 estimates the annual rate of occurrence of individual ruptures using a parallel simulated annealing algorithm known as the "Grand Inversion" (Page *et al.*, 2014). However, the large number of ruptures and the large number of solutions make UCERF3 a challenge to use for site-specific analyses.

Previously, Biasi and Anderson (2016) showed that the magnitude-frequency distribution of the UCERF3 ruptures that use the subsection closest to the Lovejoy Buttes site can closely approximate the USGS NSHM total hazard. In particular, using the rupture rates of only that one closest subsection recovers nearly all of the hazard at the Lovejoy Buttes site at the long return periods for which the PBRs provide ground-motion constraints. In addition, Anderson & Biasi (2016) showed that >98% of ruptures that include the adjacent subsections to that one closest subsection to the Lovejoy Buttes site also rupture that closest subsection, which suggests that the ruptures that dominate the hazard on the Mojave South section are large, through-going ruptures.

Informed by both of these key results of Biasi and Anderson (2016), for our SSC model of Lovejoy Buttes we used the UCERF3 magnitude frequency distributions for the participation rate of the San Andreas fault Mojave South section (Table A1). Specifically, we used the weighted mean on-fault sub-seismogenic and supra-seismogenic participation rate of the San Andreas fault Mojave South section. However, only the minimum and maximum participation rates are provided as the uncertainty on the weighted mean rate. Due to the inverse correlation between participation of segments at high and low magnitudes, it is not appropriate to use these minimum and maximum participation rates as epistemic uncertainty on the magnitude-frequency distribution on the fault section. Instead, we know that the minimum and maximum provide limits on the scaling of the median estimate. We selected to apply a symmetric epistemic uncertainty on the weighted mean participation rates as a sensitivity analysis on the effect of the rupture rates on the PBR validation results.

Lovejoy Buttes ground-motion characterization

We selected a partially nonergodic suite of GMMs in our GMC model, in order to use the site-specific hazard constraints provided by the PBRs to validate the ground-motion estimates for the Lovejoy Buttes site. We, therefore, considered systematic source and site effects for a given earthquake scenario on the San Andreas fault and the location of the Lovejoy Buttes site. Relative to ergodic hazard estimates, nonergodic hazard analyses often reduce ground motions at long return periods. However, epistemic uncertainties often increase in nonergodic hazard analyses due to the sparse ground-motion data to constrain the source- and site-specific effects.

The Southwestern U.S. (SWUS) GMC project was conducted to meet the requirements of a SSHAC Level 3 seismic hazard study (GeoPentech, 2015). A SSHAC Level 3 approach is a formal, structured methodology to provide reasonable regulatory assurance that the center, body, and range (CBR) of the technically defensible interpretations (TDI) in the GMC models have been adequately captured for use in PSHA (Hanks *et al.*, 2019; SSHAC, 1997; SSHAC, 2012). This refers to the complete characterization of uncertainty in present-day technical knowledge, available data, methods, and models. The end result of a SSHAC Level 3 study is reproducible, defensible, transparent, and stable ground-motion estimates. Specifically, the SWUS GMC project resulted in an alternative set of site-specific GMMs to be used in PSHAs of nuclear power plants in California (Diablo Canyon Power Plant – DCPP) and Arizona (Palo Verde Nuclear Generating Station – PVNGS).

The SWUS GMC project developed a new method for the median and the total aleatory standard deviation and to capture the epistemic uncertainty range of magnitude and distance scaling in GMMs as a continuous distribution. First a common functional form was fitted to the suite of applicable GMMs, which was then both interpolated between and extrapolated beyond the range of the input GMMs. The developed covariance matrix for the distributions of coefficients of the common-form models was then used to generate a large suite of these common-form GMMs. A Sammon's map representation based on the of the alternative magnitude and distance scaling was used to approximate the standard deviation between any two models. This continuous distribution of GMMs which can then be discretized into representative models that are mutually exclusive and collectively exhaustive, to better capture the center, body and range of median GMM estimates. Importantly, the weights assigned to the alternative models within a logic tree format are probabilities based on discretizing continuous distribution, rather than relative merit weights.

The SWUS GMMs use a total sigma model (σ), which uses the total standard deviation of the combined with-event (ϕ) and between-event (τ) components of the aleatory variability. A

simplified logic tree of three representative branches is used for the total sigma model to reduce the number of models for the hazard calculation while still capturing the original distribution of the total sigma. The SWUS models use a single-site within-event standard deviation model (ϕ_{SS}) which is a partially nonergodic approach that removes the systematic site effects from the traditional ergodic within-event standard deviation (Rodriguez- Marek *et al.*, 2014). Therefore, this systematic site effect for the Lovejoy Buttes site needs to be determined.

For our Lovejoy Buttes GMC model, we used the SWUS common-form Model A, which is based on rupture distance, and the GMM coefficients developed for DCPP because of the strike-slip style of faulting and large magnitude earthquakes at short distances dominating the hazard. The style of faulting flags in the common-form model were both set to zero, due to the strike-slip motion on the San Andreas fault. We used the DCPP coefficients for a period of 0.01 s, because 0.01 s is considered representative of the PGA at our site (Table A2). The result is 23 models that produce a hazard estimate (Figure 2). We used the published weights of these common-form models, as well as the total sigma values and branch weights.

Next, we determined the site-to-site residual, or site term, and uncertainty for the Lovejoy Buttes site, to not only calculate the necessary scaling to the ground-motion estimates but also the necessary epistemic uncertainty in the GMC model. To achieve this, we first filtered the NGA-West2 ground-motion database (Bozorgnia *et al.*, 2014) to stations located in California and also the subset of data used by the four NGA-West GMMs ASK14 (Abrahamson *et al.*, 2014), BSSA14 (Boore *et al.*, 2014), CB14 (Campbell & Bozorgnia, 2014), and CY14 (Chiou & Youngs, 2014). We then calculated the total residual between the recorded PGA and the PGA estimated by each of the four NGA-West2 GMMs. We then fitted a linear mixed-effects model to separate the station-effects of interest from the event-effects within the total residual for each of the four NGA-West2 GMMs.

We then estimated the spatial correlation of the station-effects using an empirical semivariogram to measure the dissimilarity of two observed station-effect values. We assumed that all stations separated by the same distance have the same semivariance, and so could group all observations with the same separation distance to estimate the semivariance. Specifically, we considered stations with a maximum separation distance of 80 km and grouped the separation distances of the stations in 1 km bins. The 1 km bins were chosen to result in a reasonable number of site pairs in each bin, while avoiding mixing site pairs with differing distances. We calculated an empirical semivariogram for each of the four NGA-West2 GMMs. For each of the four empirical semivariograms, we then fitted a semivariogram model using an exponential model (Jayaram & Baker, 2009).

$$\gamma(h) = C_0 + a[1 - \exp(-3h/b)] \quad (1)$$

In Equation 1, $\gamma(h)$ is the correlation between two stations, C_0 is the nugget effect (a constant value for all distances greater than zero, therefore the y-axis intercept), h is the scalar distance between the two stations, and a and b are the sill (the variance of the random variable; PGA) and range (the separation distance h at which $\gamma(h)$ equals 0.95 times the sill) of the semivariogam function (Table A3). Figure 3a shows the good fit of the empirical data to the fitted exponential semivariogram, particularly at short distances where it is most important to model the semivariogram structure because this is where correlations are greatest. It is important to note the significant impact of the nugget effect in dropping the correlations at short separation distances to ensure this good match.

We then made a conditional prediction of the site term at the Lovejoy Buttes site, using the stations within a 30 km radius of Lovejoy Buttes (Figure 1). The station-residuals at these stations closest to Lovejoy Buttes are shown in Figure 3b. For these stations, a correlation matrix and a covariance matrix were defined for each NGA-West2 model (Stafford, 2012). The conditional mean of the site term at Lovejoy Buttes, conditional variance, and conditional standard deviation were calculated. We used the mean site term of the four NGA-West2 models and the mean standard deviation. The reliability of the station-residual estimated for each station is partly accounted for in the nugget effect, however, we additionally sample the standard error of the station-residual and added this standard deviation to the mean conditional standard deviation.

Our logic tree mean site term for Lovejoy Buttes has a value of 0.22, which results in an amplification of the PGA estimates. The standard deviation on this mean of 0.4 results in our logic tree high and low site term branches having values of 0.62 and -0.18, respectively. Therefore, while the high site term branch produces a significant amplification of PGA at Lovejoy Buttes, the low site term branch results in deamplification of PGA at Lovejoy Buttes. With this final piece of information added to the logic tree, our PSHA model can be run to calculate the hazard at the Lovejoy Buttes site for each combination of logic tree branches. The 23 base model branches, three site term branches, and three sigma branches result in 207 realizations through our GMC model logic tree (Figure 2).

Hazard Validation and Updating

The idea that, in theory, the probability that a PBR would have survived to the present day, assuming a given hazard result, is equal to the confidence level of the PSHA model inputs to that given hazard estimate was established decades ago (Anderson & Brune, 1999a). However, in practice, methods to implement and apply this idea have only been developed more recently (Baker *et al.*, 2013; Hanks *et al.*, 2013; Rood *et al.*, 2020). The PSHA model, without any constraints from

the PBR data, outputs a suite of hazard curves, λ_i. The weight of each hazard curve, $P(\lambda_i)$, reflects the product of logic tree branch weights from the origin of the logic tree to the terminal node (Figure 2). The suite of $[\lambda_i, P(\lambda_i)]$ collectively defines a discrete probability distribution. It is important to note that the individual hazard curves can cross each other, or change their relative position with variations in PGA, but the weights remain constant for all PGA levels. Here, we individually validated each hazard curve output by our PSHA model, to update the associated weight of each hazard curve informed by the observation that the PBRs at Lovejoy Buttes remain standing.

First, we constructed a PGA-based fragility function for the probability of failure of each Lovejoy Buttes PBR. We use PGA because it is the most relevant ground-motion parameter for short-period shaking that is likely to affect PBRs. To calculate the fragility functions, we used the Lovejoy Buttes measured PBR geometric factors of Rood *et al.* (*2022*)(Table 1), the probability of toppling equations of Purvance *et al.* (2008a) and the methods of Rood *et al.* (2020). LJ5 has a symmetric geometry and therefore the Purvance *et al.* (2008a) symmetric rocking response equation was used, whereas LB05, LJB1, LJB2, and LJ1 have asymmetric geometries and therefore the Purvance *et al.* (2008a) asymmetric rocking response equation was used. The Purvance *et al.* (2008a) equations give the probability of toppling a PBR for a given pair of PGA and PGV/PGA values. PGA is the amplitude of the ground-motion excitation force on the PBR and PGV/PGA relates to the waveform of the ground motion and so is the period of time during which a PBR is forced to tip in one direction. For each value of PGA investigated, the distribution of PGV/PGA was calculated using a conditional GMM for PGV that is based on the PGA (Abrahamson & Bhasin, 2020). A single magnitude of 8 Mw and a distance of 15.2 km was used to calculate the PGV/PGA distribution for all PGA values. These values are the modal disaggregation magnitude and distance calculated by the USGS Unified Hazard Tool for the Lovejoy Buttes site at a return period of 2475 years. The use of a single magnitude and distance is appropriate given that the San Andreas fault is the single seismic source to the Lovejoy Buttes site. The median probability of toppling across the PGV/PGA distribution was calculated for each PGA intensity to produce the fragility function for each PBR based on PGA only (Figure 4). The slopes of the calculated fragility functions in Figure 4 reflect the variability of the seismic capacity of each PBR, and the influence of PGV on the failure of the PBR is reflected in that variability.

However, the PBR fragility and hazard validation methods of Rood *et al.* (2020) do not provide an estimate of uncertainty on the fragility function of each Lovejoy Buttes PBR. Therefore, to incorporate uncertainty in the fragility of each PBR in our hazard validation, we assumed a log-normally distributed uncertainty as a discrete 3-point approximation. A weight of 0.3, 0.4, and 0.3

(1.28σ) were applied to the lower, central, and upper fragility levels of each PBR, respectively. An uncertainty of 0.2 log units was applied to the PBRs that Rood *et al.* (*2022*) considered to have a high confidence in their fragility characterization (LB05, LJ1, and LJ5) and 0.3 log units was applied to the PBRs that have only a moderate confidence in their fragility calculation (LJB1 and LJB2). These two alternative values are to account for the varying degrees of confidence in the fragility characterization of the PBRs by the equations on Purvance *et al.* (2008a). The hazard validation was conducted three times for each PBR, once for each of the fragility levels in 3-point uncertainty approximation, and the weighted mean used for each PBR.

We validated each hazard curve output from our PSHA model with the fragility function of each PBR to determine which hazard curves are most consistent with the observation of PBR survival using the methods of Rood *et al.* (2020). The fragility function provides the probability of failure of a given PBR (PBR_j) for a given PGA intensity, $P(Failure|PGA = a;\ PBR_j)$. To compute the PBR probability of survival for a given hazard curve, $P(\lambda_i \mid PBR_{s,j})$, we need to first convolve the hazard curve, specifically the derivative of the hazard curve, with the fragility function of the PBR (Equation 2).

$$\lambda_{Failure} = \int P(Failure|PGA = a;\ PBR_j).\left|\frac{d\lambda_i(a)}{da}\right| da \quad (2)$$

We then assume that $P_{Failure} \approx \lambda_{Failure}$ and a Poisson occurrence to determine the annual probability of failure:

$$P_{Failure} = 1 - e^{-\lambda_{Failure}} \quad (3)$$

The probability of survival of a PBR from its fragility age to the present time given a hazard estimate is then found from:

$$P(\lambda_i \mid PBR_{s,j}) = e^{-P_{Failure}.t} \quad (4)$$

Previous PBR hazard validation methods have only used the median fragility age of a PBR and not accounted for the uncertainty in this fragility age. Instead, we improved on previous methods and accounted for the uncertainty in all, n_t, Monte Carlo realizations of fragility age, t_k ,output from the model of Balco *et al.* (2011) and updated by Rood *et al.* (*2022*). We then calculated the mean probability of survival of a PBR over the entire distribution of fragility ages:

$$P(\lambda_i \mid PBR_{s,j}) = \frac{1}{n_t}\sum_k e^{-P_{Failure}.t_k} \quad (5)$$

Similarly to the PBR hazard validation study of Rood *et al.* (2020), there is the survival of multiple PBRs at the Lovejoy Buttes site. However, in the study of Rood *et al.* (2020) all seven of the PBRs were assigned the same fragility age, so the only the most fragile PBR was used to provide the

hazard constraints. In contrast, the five Lovejoy Buttes PBRs have a range of fragility ages and fragilities. Therefore, we include the distribution of fragility age and fragility of this PBR population and use the joint probability of survival of all five PBRs to validate the hazard curves. We, therefore, define the probability of survival of multiple PBRs as $\boldsymbol{PBR_s}$.

Another notable improvement on the previous methods of Rood et al. (2020; 2022) is that we did not use the hazard curve rejection criteria of a less than 5% probability of survival (equivalent to a greater than 95% probability of failure). Instead, we considered the information provided by all resulting probabilities of survival in updating our PSHA model. Specifically, we apply the Bayesian approach of using the new observational data of the probability of survival of the PBRs at Lovejoy Buttes to update the prior distribution of logic tree end-branch weights (Equation 6). This Bayesian approach does not accept or reject hazard estimates, as is the case with the Rood et al. (2020; 2022) rejection criteria, but retains all the hazard estimates simply with updated weights.

$$P(\lambda_i \mid \boldsymbol{PBR_s}) = \frac{\left[\prod_j P\left(PBR_{s,j}|\lambda_i\right) P(\lambda_i)\right]}{\sum_j\left[\prod_j P\left(PBR_{s,j}|\lambda_i\right) P(\lambda_i)\right]} \quad (6)$$

For the Bayesian updating, $\prod_j P(\boldsymbol{PBR_s}|\lambda_i)$ is the likelihood function that represents the joint probability of survival of the PBRs given a particular hazard curve. The denominator in Equation 6 is simply a normalization factor such that the sum of the posterior, updated weights again equal 1. $P(\lambda_i \mid \boldsymbol{PBR_s})$ was calculated for each of the three fragility levels and the weighted mean was then used as the final weights for each hazard curve, $P(\lambda_i)'$. Intuitively, the hazard estimates that are most consistent with the PBR observational data, i.e., the hazard estimates with the highest PBR probability of survival, will have their weights increased. These hazard estimates will be those with lower ground motions levels. Conversely, the hazard estimates that are least consistent with the PBR observational data, i.e., the hazard estimates with the lowest PBR probability of survival, will have their weights decreased. These hazard estimates will be those with higher ground motions levels.

RESULTS

In Figure 5, the spread of the PSHA output hazard curves, due to the epistemic uncertainty captured in the GMC model logic tree, can be seen as well as the computed mean and fractile hazard curves for the Lovejoy Buttes site. At the annual frequency of exceedance of $1x10^{-4}$ yr^{-1}, which is equivalent to return period of 10,000 years, the original PSHA model estimates a mean PGA intensity of 1.47 g. The 5^{th} – 95^{th} fractile uncertainty range on this value is 0.59 – 2.14 g. Such a large uncertainty range is in part due to the considerable epistemic uncertainty in the nonergodic site term. Meanwhile, our PSHA model with PBR updated weights estimates a mean PGA intensity

of 0.52 g and the 5^{th} – 95^{th} fractile uncertainty range on this value is 0.28 – 0.60 g. Consequently, the PBR validation has resulted in a significant 65% reduction in the mean hazard estimate and a 72% reduction in the 5^{th} – 95^{th} fractile uncertainty range.

The updated end-branch weights range from 0.17 for the hazard estimate most consistent with the PBR data to 2.81×10^{-30} for the hazard estimate least consistent with the PBR data. In the updated hazard estimates informed by the PBR validation, 18 of the 207 end-branch hazard curves have updated weights of >0.01. The significant increase in the weights of these few end-branches is intrinsically associated with the significant decrease in weights of other end-branches. The weights of these 18 end-branch hazard curves account for ~90% of the total, therefore, these 18 end-branches are defining the updated hazard estimate for the Lovejoy Buttes site.

Only four of the SWUS models are used by logic tree branch combinations that have an updated end-branch weight of >0.01: Model 28, Model 29, Model 30, and Model 31. The SWUS model that performed best was Model 31. Five of the nine hazard estimates that used this branch of the logic tree have an updated weight of >0.01. The end-branch weights of the nine hazard estimates that use Model 31 sum to ~0.41. Therefore, nearly half the updated hazard estimate is determined by this model. Interestingly, in the original model with no PBR-constraints Model 31 had a weight of 0.026, which was relatively low compared to the other model branches. Intuitively, the hazard curves that used the low site term and low total sigma logic tree branches had updated weights higher than those that used the mean/central branches, which were weighted higher than those that used the high branches. In particular, the hazard estimates that used the high site term branch were down weighted to the lowest values.

DISCUSSION

In order for independent observational data to deliver an updated and improved hazard estimate, two key assumptions need to be made, which we, therefore, made in our study. First, it is assumed that the prior PSHA model was executed to a sufficiently rigorous standard, since updating a prior sub-standard PSHA model would not resolve the inherent issues therein. Second, it is assumed that the conversion of the original observational data (i.e., the PBR) into the parameters used to validate and update the PSHA model (i.e., fragility and fragility age) was conducted to a rigorous standard and the appropriate level of uncertainty included. Below we discuss the uncertainty and sensitivity in both of these assumptions, and the associated impacts on the updated hazard estimates.

PSHA model uncertainty

SSC model uncertainty

We conducted a sensitivity analysis on our SSC model rupture rates by scaling the UCERF3 weighted mean Mojave South section participation rates within the maximum and minimum uncertainty bounds. We scaled the participation rates equally across all magnitudes; therefore, the shape of the hazard curves was unchanged, and the hazard curves simply translated vertically. In order to satisfy the slip constraints of the UCERF3 inversion, if the participation rate, and therefore, the moment rate, is increased at one magnitude, it is necessary to have an equal decrease in moment rate at other magnitudes. However, we did not have the necessary information to make such trading of moment rate between different magnitudes. Therefore, our analysis is just a first-order sensitivity analysis of the effect on rupture rates on our hazard validation.

At the previously considered annual frequency of exceedance, $1x10^{-4}$ yr^{-1}, the scaling of the participation rates had a minor effect on the original PSHA model mean hazard estimate: 1.47 g with weighted mean participation rates, 1.30 g and 1.58 g with the scaled downwards and upwards participation rates, respectively. This minor difference in the original PSHA hazard estimates resulted in a negligible difference in the PBR-informed hazard estimates: 0.52 g with weighted mean participation rates, 0.52 g and 0.53 g with the scaled downwards and upwards participation rates, respectively. Therefore, we conclude that, to the first order, the range of participation rates that we are able to investigate cannot explain the inconsistency between the hazard estimates and PBR survival. However, in future studies, at Lovejoy Buttes and elsewhere, the use of a SSC model with a logic tree that considers the full epistemic uncertainty in earthquake rupture rates is recommended.

GMC model uncertainty

In the GMC model, epistemic uncertainty in the SWUS project is included as the distribution of coefficients for the common-form model, i.e., the 23 DCPP models. In addition, the partially nonergodic single-station sigma approach results in a reduced aleatory variability but an increased epistemic uncertainty in the GMMs because of the limited data to constrain site term for Lovejoy Buttes. The GMC model logic tree explicitly accounts for the epistemic uncertainty in the common-form models, site term, and total sigma. In the case of the site term and total sigma, the continuous distribution of uncertainty that has been discretized into three branches that are assumed to be sufficient to capture the mean and variability of the uncertainty.

An important source of uncertainty in our PSHA model is the site term for the nonergodic GMMs. One issue is that the mean PGA intensity recorded by the PEER database stations that were used to derive the Lovejoy Buttes site terms was 0.008 g and the number of recordings at each station ranged from 1 to 49, with a mean of 12 recordings per station. The greatest PGA intensity recorded

by these stations was 0.27 g, however this was the only ground-motion record for the station. While we accounted for the number of recordings at a given station in our site term uncertainty, there were relatively few ground-motion recordings in proximity to Lovejoy Buttes to constrain this site term. In addition, we are extrapolating our Lovejoy Buttes site term to PGA intensities beyond the recorded PGA values we modeled the residuals from. However, our mean site term showing slight amplification of PGAs at Lovejoy Buttes is consistent with the results of Abbott (2001) and Stirling *et al.* (2002). Furthermore, we calculated a large uncertainty on this mean site term, which is included as epistemic uncertainty in our PSHA model.

The SWUS GMMs were developed for a reference site condition with V_{S30} (travel-time-averaged shear wave velocity in the top 30 m) of 760 ms^{-1}. Therefore, in the SWUS GMMS, there is no site term. Based on the V_{S30} map of Thompson *et al.* (2014), the V_{S30} at Lovejoy Buttes is 717 ms^{-1}. An uncertainty on this V_{S30} value of 0.1 log units, approximately 10% uncertainty, gives a V_{S30} range of approximately 648–785 ms^{-1} at Lovejoy Buttes. Therefore, the reference site V_{S30} of 760 ms^{-1} is within the uncertainty that V_{S30} can be resolved at Lovejoy Buttes. Scaling in ground motions over the difference between 760 ms^{-1} and 717 ms^{-1} will have a negligible impact on the ground-motion estimates. Therefore, for our study it was not necessary to produce a robust site-specific V_{S30} adjustment to the SWUS GMMs.

PBR uncertainty

Our method of considering the joint probability of survival of all five PBRs provides a much stronger test than considering the survival of just a singular PBR. In addition, we demonstrated that our analysis is not dominated by the probability of survival of a particular one of the five Lovejoy Buttes PBRs. We conducted a leave-one-out sensitivity analysis that showed that at an annual frequency of exceedance $1x10^{-4}$ yr^{-1} the updated hazard curves using the constraints of only four out of the five PBRs ranges only 0.05 g. Therefore, by considering the constraints provided by all five PBRs, are results are insensitive to the survival of a single PBR.

Fragility uncertainty

We accounted for uncertainty in the fragility functions of the PBRs and, importantly, that this uncertainty varies from PBR to PBR. However, it is also important to note that we only investigated uncertainty in the median of the fragility function but did not consider uncertainty in the variability. In principle, it is necessary to account for three sources of uncertainty in the median fragility functions of the PBRs. First, there is uncertainty in whether the model is correct for the data it is fitting. We have only considered one fragility model derived from the experimental block toppling data, so there is no epistemic uncertainty on what the appropriate model to this data should be.

Second, given the fragility model of Purvance *et al.* (2008a) to describe the data, there is parametric uncertainty in the optimal coefficients of this model. Purvance *et al.* (2008a) provides the model median and 95% confidence interval predictions, which provide some information on this parametric uncertainty. Third, there is uncertainty in whether the data and model for the rectangular blocks investigated by Purvance *et al.* (2008a) are representative of the PBRs that we are modeling with the fragility equations.

While the equation provided for the 95% confidence interval gives some quantification of the parametric uncertainty in the model of Purvance *et al.* (2008a) an assumption would have to be made about the underlying distribution of uncertainty in order to fit a model to this uncertainty. In addition, we have to assume a value for the other two sources of uncertainty, for which there is no available constraints on these values. Therefore, we decided to assume a single uncertainty value that is large enough to consider all three sources of uncertainty in a PBR fragility function. We assumed a log-normally distributed uncertainty as a discrete 3-point approximation. An uncertainty of 0.2 log units was applied to the PBRs that Rood *et al.* (*2022*) considered to have a high confidence in their fragility characterization (LB05, LJ1, and LJ5) and 0.3 log units was applied to the PBRs that have only a moderate confidence in their fragility calculation (LJB1 and LJB2). These two alternative values are to account for the varying degrees of confidence in the fragility characterization of the PBRs by the equations on Purvance *et al.* (2008a).

Fragility age uncertainty

We improved on previous PBR hazard validation methods and explicitly accounted for the full range of modeled uncertainty in the fragility age of each PBR. We included the uncertainty of all 400 Monte Carlo realizations of fragility age output from the model of Balco *et al.* (2011) and updated by Rood *et al.* (*2022*). Each fragility age was used to calculate 400 probabilities of survival of the PBR for a given hazard estimate. We then calculated the mean probability of survival of a PBR over the entire distribution of fragility ages. Therefore, in our analysis we account for the fact that the fragility age of some PBRs is better constrained than other PBRs.

Logic tree weights updating

In our analysis, we only updated the end-branch weight associated with each alternative combination of PSHA model logic tree branches. The updating of these end-branch weights does not affect the calculation of the exceedance rates of the ground-motion levels estimated by the output seismic hazard curves. Therefore, the updating only changes the calculated statistical hazard curves, such as the mean, median, and fractile curves. In order to update the exceedance rates of the

ground-motion levels estimated by the output seismic hazard curves, the inputs to the PSHA model would need to be updated.

It is important to appreciate that the logic- tree branch end weights result from the combination of branch weights at individual nodes across the logic tree. Therefore, the updating of the branch end weight effectively modifies each of the branch weights on the individual nodes associated with that logic tree branch. This result in the same branch of a logic- tree node having different effective weights depending on how it combines with downstream branches. Different effective weights on the same branch requires that each path through the logic tree collectively as a set of decisions or parameters associated with the hazard calculations.

In the future, a more extensive analysis could be performed at each node in the logic tree that utilizes expert judgement and the full distribution of PBR probabilities of survival at each node. In such an analysis, for the alternative branches at a node in the logic tree, the distribution of PBR probabilities of survival would be compared for all hazard estimates that use a given branch. Therefore, the PBR validation results would be considered at each individual node in turn, which would allow not only the reweighting of each branch but inform the necessary reevaluation and improvement to the model associated with each branch.

The PSHA-PBR inconsistency

There is only a small number of output hazard curves that have updated weights high enough to contribute to the calculated mean and fractile hazard curves results. Therefore, these mean and fractile hazard curves are sensitive to the discretization of our PSHA model logic tree. For this low number of hazard estimates that are consistent with PBR survival, the discretization is too sparse and so there are an insufficient number of hazard curves to calculate meaningful statistics. In our analysis, we assumed that three branches were sufficient to capture the mean and variability of a continuous uncertainty distribution. However, in light of the PBR validation results the discretization into more branches would have improved the calculation of the PBR-informed fractile hazard curves. Importantly, this increased discretization of our PSHA model would not improve the consistency of the PSHA model with the PBR data; it would only improve the calculation of statistical hazard curves.

Not only is the PBR probability of survival putting constraints on extreme ground motions at the Lovejoy Buttes site, but the age and fragility of the five PBRs are also putting constraints on ground-motion intensities that have been recorded of historical earthquakes in California. For example, ~0.57 g was recorded during the 2019 7.1 Mw Ridgecrest earthquake at a distance of ~3 km. This recently recorded level of ground shaking is approximately the mean ground-motion

554 estimate for the 1 in 10,000 year earthquake at Lovejoy Buttes. However, unlike the Ridgecrest
555 earthquake, the Lovejoy Buttes site is located only 15 km from the San Andreas fault.

556 There has been known shaking, but at some unknown level, at the Lovejoy Buttes site during the
557 historic 1812 Wrightwood and 1857 Fort Tejon earthquakes, as well as prehistoric earthquakes
558 recorded in the paleo-seismic data at Wrightwood and Pallet Creek. The historical recorded damage
559 to the San Gabriel mission during both the 1812 Wrightwood and 1857 Fort Tejon earthquakes has
560 the potential to place empirical constraints on the ground-motion estimates of historical ruptures on
561 the Mojave South section of the San Andreas fault. The San Gabriel mission is located ~45 km from
562 the Mojave South section of the San Andreas fault. The San Gabriel mission historical descriptions
563 estimate damage at a Modified Mercalli intensity (MMI) VII for both the 1812 Wrightwood and
564 1857 Fort Tejon earthquakes (Toppozada *et al.*, 2002). The MMI-PGA relationship of Wald *et al.*
565 (1999) provides a PGA estimate of 0.18 – 0.34 g at the San Gabriel mission for this intensity of
566 damage. This PGA range is consistent with the PBR constraints on ground-motion estimates at
567 Lovejoy Buttes. A more sophisticated analysis of the ground-motion estimate for San Gabriel
568 damage could be conducted in a similar manner as the analysis of the toppling of locomotives
569 (Anooshehpoor *et al.*, 1999; Veeraraghavan *et al.*, 2019).

570 Anomalously low ground-motions during the historical 1812 Wrightwood and 1857 Fort Tejon
571 earthquakes has been previously proposed to be due to directivity effects produced by interactions
572 between the San Andreas fault and San Jacinto fault (Grant Ludwig *et al.*, 2015). Dynamic rupture
573 modeling has investigated the potential for these proposed low ground motions at PBR sites in
574 southern California (Lozos *et al.*, 2015; Olsen & Brune, 2008). These studies concluded that long
575 unilateral rupture of the San Andreas fault within the last few thousand years since the PBRs
576 became fragile was unlikely, and that instead ruptures likely either initiated or terminated at the
577 stepover junction between the San Andreas and San Jacinto fault in Cajon Pass. These studies
578 demonstrate how PBR data can be used as a validation of both PSHA and physics-based models.

579 One potential interpretation of the PBR validation results at Lovejoy Buttes is that, despite our first-
580 order sensitivity analysis, the rupture rates for the Mojave South section of the San Andreas fault
581 are significantly too high. However, if the rupture rates on the San Andreas are reduced then strain
582 and energy release will need to be placed elsewhere within the UCERF3 model, which will increase
583 the rupture rates on other faults. These smaller faults in UCERF3 will need to have significantly
584 increased slip rates and so significantly shorter recurrence intervals of large earthquakes. Therefore,
585 the results at Lovejoy Buttes potentially have implications across California. However, this
586 repartitioning is limited to the temporal variation of slip rates on the San Andreas fault constraints

from the paleoseismic studies that go into UCERF3, both on the San Andreas and other surrounding faults.

A potential alternative interpretation of the PBR validation results at Lovejoy Buttes is that the cause of the inconsistent ground-motion results from the GMC model. The epistemic uncertainty between the end-branch hazard curves that have weights >0.01 is too low to accurately reflect the true level of confidence in the GMC model. The level of inconsistency between PBR survival and the original PSHA estimates suggest that reweighing the end-branches of the model is not appropriate. Instead, rather than simply reweighting the existing hazard curves, a new GMC model should be developed for the Lovejoy Buttes site, which estimate ground motions at rates of exceedance that are compatible with the PBR data. It is essential that the PSHA model produces a distribution of hazard estimates that are consistent with a high probability of PBR survival in order have appropriate epistemic uncertainty in the hazard estimates. Otherwise, the few remaining highest-weighted hazard curves will result from the least geologically probable branches in the SSC model because inappropriate GMC models were used. It has previously been proposed that the decrease in sigma that can be achieved by eliminating the ergodic assumption in GMMs would eliminate the inconsistency between the PBR survival and hazard estimates at Lovejoy Buttes (Anderson *et al.*, 2014; Anderson & Brune, 1999b). It is important to recall that these SWUS GMMs are partially nonergodic and so already have a reduced aleatory variability compared to conventional ergodic GMMs. However, this partially nonergodic single-station approach has been shown to remove 30% of the aleatory variability of the ergodic model, compared to 60%–70% for a fully nonergodic model (Abrahamson *et al.*, 2019).

CONCLUSIONS

We performed a validation of earthquake hazard estimates for the Mojave South section of the San Andreas fault using ground-motion constraints on past earthquakes provided by the survival of ancient PBRs. We used the state-of-the-art SSC model for southern California, UCERF3, and the partially nonergodic GMC model developed for nuclear facilities in the southwestern U.S., SWUS GMMs, to construct a PSHA model for the PBR site. A fragility function was calculated for each PBR, which were then used to validate each alternative logic tree hazard estimate for the site by calculating the probability of survival of the PBR given each hazard estimate. Importantly, in our analysis we considered the joint probability of survival of the five studied PBRs, as well as uncertainty in both the fragility and fragility age characterization of each PBR. Bayesian updating was used to reweight the earthquake hazard estimates using the calculated probability of survival of the PBRs for each hazard estimate.

620 At an annual frequency of exceedance of $1x10^{-4}$ yr^{-1}, equivalent to a return period of 10,000 years,
621 the mean hazard estimate was significantly reduced by 65%. The 5^{th}-95^{th} fractile uncertainty range
622 was reduced by 72% and few hazard curves remain that contribute to the hazard estimate for the
623 site. The magnitude of this inconsistency is difficult to rectify in the SSC model or GMC model
624 individually, therefore, both components of our PSHA model need to be examined. While the
625 PSHA earthquake hazard estimates for Lovejoy Buttes are drastically inconsistent with our PBR
626 data, this result is notably consistent with the findings of previous PBR studies at Lovejoy Buttes
627 (Anderson *et al.*, 2014; Purvance *et al.*, 2008b). These previous PBR studies all identified the
628 sizeable apparent overestimation of earthquake ground shaking at Lovejoy Buttes over the timescale
629 of tens of thousands of years; however these previous studies used deterministic fragilities, had no
630 fragility age constraints, and no logic trees to interrogate. Importantly, our analysis is the first to
631 rigorously validate a site-specific PSHA model for Lovejoy Buttes, utilizing recent advancements in
632 both PSHA models and PBR fragility and fragility age models.

633 Our results are compelling evidence that hazard estimates for the San Andreas fault, especially for
634 rare, large earthquakes, are undeniably incompatible with geologic evidence at Lovejoy Buttes. This
635 potentially has important implications for the earthquake hazard estimates of Los Angeles, because
636 the Mojave South section of the San Andreas fault contributes significantly to the hazard from rare,
637 large earthquakes for both Lovejoy Buttes and Los Angeles. Crucially, our results add to the
638 cumulative weight of evidence regarding the valuable independent observation data provided by
639 PBRs to validate ground-motion estimates in seismically active regions both in California and
640 globally.

641 **DATA AND RESOURCES**

642 The UCERF3 magnitude frequency distributions for the participation rates were retrieved from
643 http://opensha.usc.edu/ftp/UCERF3.3/Model/FaultMFDs/ParticipationIncremental/ (last accessed
644 April 2023). The SWUS DCPP GMM coefficients were retrieved from
645 http://www.lettisci.com/sshac3/SWUS_GMC_TR_Appendices.zip (last accessed April 2023). All
646 other data used in this paper came from published sources listed in the references.

647 **DECLARATION OF COMPETING INTERESTS**

648 The authors declare no competing interests.

649 **ACKNOWLDEGEMNETS**

650 Funding for this work was provided by Southern California Earthquake Center (SCEC) Award no.
651 09113, 1070, 12088, 13062, a Lawrence Livermore National Laboratory Lawrence Scholar

652 Program Fellowship (to Dylan Rood), NSF Postdoctoral Fellowship Award no. EAR-0948350 (to
653 Dylan Rood, and a studentship provided by the EPSRC Doctoral Training Partnership no.
654 EP/N509486/1 (to Anna Rood). This is SCEC contribution number 13369. We are grateful to three
655 anonymous reviews for their thoughtful feedback, which greatly improved the manuscript.

656 **REFERENCES**

657 Abbott, R. E. (2001). *Geophysical Constraints on Seismic Hazard and Tectonics in the Western Basin and*
658 *Range* University of Nevada, Reno.].
659 https://scholarworks.unr.edu/bitstream/handle/11714/1083/Mackay001_Abbott.pdf?sequence=1
660 &isAllowed=y
661 Abrahamson, N. A., & Bhasin, S. (2020). *Conditional ground-motion model for peak ground velocity for*
662 *active crustal regions. PEER Report No. 2020/05*.
663 https://peer.berkeley.edu/sites/default/files/publications/2020_05_abrahamson_final.pdf
664 Abrahamson, N. A., Kuehn, N. M., Walling, M., & Landwehr, N. (2019). Probabilistic Seismic Hazard Analysis
665 in California Using Nonergodic Ground-Motion Models. *Bulletin of the Seismological Society of*
666 *America*, *109*(4), 1235-1249. https://doi.org/10.1785/0120190030
667 Abrahamson, N. A., Silva, W. J., & Kamai, R. (2014). Summary of the ASK14 Ground Motion Relation for
668 Active Crustal Regions. *Earthquake Spectra*, *30*(3), 1025-1055.
669 https://doi.org/10.1193/070913eqs198m
670 Ancheta, T. D., Darragh, R. B., Stewart, J. P., Seyhan, E., Silva, W. J., Chiou, B. S. J., Wooddell, K. E., Graves, R.
671 W., Kottke, A. R., Boore, D. M., Kishida, T., & Donahue, J. L. (2014). NGA-West2 Database.
672 *Earthquake Spectra*, *30*(3), 989-1005. https://doi.org/10.1193/070913EQS197M
673 Anderson, J. G., Biasi, G. P., & Brune, J. N. (2014). Chapter 14 - Precarious Rocks: Providing Upper Limits on
674 Past Ground Shaking from Earthquakes. In J. F. Shroder & M. Wyss (Eds.), *Earthquake Hazard, Risk*
675 *and Disasters* (pp. 377-403). Academic Press. https://doi.org/https://doi.org/10.1016/B978-0-12-
676 394848-9.00014-6
677 Anderson, J. G., & Brune, J. N. (1999a). Methodology for using Precarious Rocks in Nevada to test seismic
678 hazard models. *Bulletin of the Seismological Society of America*, *89*.
679 https://doi.org/10.1785/BSSA0890020456
680 Anderson, J. G., & Brune, J. N. (1999b). Probabilistic Seismic Hazard Analysis without the Ergodic
681 Assumption. *Seismological Research Letters*, *70*(1), 19-28. https://doi.org/10.1785/gssrl.70.1.19
682 Anderson, J. G., Brune, J. N., Biasi, G., Anooshehpoor, A., & Purvance, M. (2011). Workshop Report:
683 Applications of Precarious Rocks and Related Fragile Geological Features to U.S. National Hazard
684 Maps. *Seismological Research Letters*, *82*(3), 431-441. https://doi.org/10.1785/gssrl.82.3.431
685 Anooshehpoor, A., Brune, J. N., & Zeng, Y. (2004). Methodology for Obtaining Constraints on Ground
686 Motion from Precariously Balanced Rocks. *Bulletin of the Seismological Society of America*, *94*(1),
687 285-303. https://doi.org/10.1785/0120020242
688 Anooshehpoor, A., Heaton, T. H., Shi, B., & Brune, J. N. (1999). Estimates of the ground accelerations at
689 Point Reyes Station during the 1906 San Francisco earthquake. *Bulletin of the Seismological Society*
690 *of America*, *89*(4), 845-853. https://doi.org/10.1785/bssa0890040845
691 Atik, L. A., Abrahamson, N., Bommer, J. J., Scherbaum, F., Cotton, F., & Kuehn, N. (2010). The Variability of
692 Ground-Motion Prediction Models and Its Components. *Seismological Research Letters*, *81*(5), 794-
693 801. https://doi.org/10.1785/gssrl.81.5.794
694 Atkinson, G. M. (2006). Single-Station Sigma. *Bulletin of the Seismological Society of America*, *96*(2), 446-
695 455. https://doi.org/10.1785/0120050137
696 Atkinson, G. M., Bommer, J. J., & Abrahamson, N. A. (2014). Alternative Approaches to Modeling Epistemic
697 Uncertainty in Ground Motions in Probabilistic Seismic-Hazard Analysis. *Seismological Research*
698 *Letters*, *85*(6), 1141-1144. https://doi.org/10.1785/0220140120
699 Baker, J. W., Abrahamson, N. A., Whitney, J. W., Board, M. P., & Hanks, T. C. (2013). Use of Fragile Geologic
700 Structures as Indicators of Unexceeded Ground Motions and Direct Constraints on Probabilistic

Seismic Hazard Analysis. *Bulletin of the Seismological Society of America*, *103*(3), 1898-1911. https://doi.org/10.1785/0120120202

Baker, J. W., Bradley, B., & Stafford, P. J. (2021). *Seismic Hazard and Risk Analysis*. Cambridge University Press. https://doi.org/10.1017/97811082425056.010

Balco, G., Purvance, M. D., & Rood, D. H. (2011). Exposure dating of precariously balanced rocks. *Quaternary Geochronology*, *6*(3), 295-303. https://doi.org/10.1016/j.quageo.2011.03.007

Biasi, G., & Anderson, J. G. (2016). Disaggregating UCERF3 for Site-Specific Applications. *Earthquake Spectra*, *32*(4), 2009-2026. https://doi.org/10.1193/071515EQS114M

Biasi, G. P., Weldon, R. J., II, Fumal, T. E., & Seitz, G. G. (2002). Paleoseismic Event Dating and the Conditional Probability of Large Earthquakes on the Southern San Andreas Fault, California. *Bulletin of the Seismological Society of America*, *92*(7), 2761-2781. https://doi.org/10.1785/0120000605

Bommer, J., & Abrahamson, N. A. (2006). Why Do Modern Probabilistic Seismic-Hazard Analyses Often Lead to Increased Hazard Estimates? *Bulletin of the Seismological Society of America*, *96*, 1967-1977. https://doi.org/10.1785/0120060043

Boore, D. M., Stewart, J. P., Seyhan, E., & Atkinson, G. M. (2014). NGA-West2 Equations for Predicting PGA, PGV, and 5% Damped PSA for Shallow Crustal Earthquakes. *Earthquake Spectra*, *30*(3), 1057-1085. https://doi.org/10.1193/070113eqs184m

Bozorgnia, Y., Abrahamson, N. A., Atik, L. A., Ancheta, T. D., Atkinson, G. M., Baker, J. W., Baltay, A., Boore, D. M., Campbell, K. W., Chiou, B. S.-J., Darragh, R., Day, S., Donahue, J., Graves, R. W., Gregor, N., Hanks, T., Idriss, I. M., Kamai, R., Kishida, T., . . . Youngs, R. (2014). NGA-West2 Research Project. *Earthquake Spectra*, *30*(3), 973-987. https://doi.org/10.1193/072113eqs209m

Brune, J. N. (1996). Precariously balanced rocks and ground-motion maps for Southern California. *Bulletin of the Seismological Society of America*, *86*(1A), 43-54.

Brune, J. N. (1999). Precarious Rocks along the Mojave Section of the San Andreas Fault, California: Constraints on Ground Motion from Great Earthquakes. *Seismological Research Letters*, *70*(1), 29-33. https://doi.org/10.1785/gssrl.70.1.29

Campbell, K. W., & Bozorgnia, Y. (2014). NGA-West2 Ground Motion Model for the Average Horizontal Components of PGA, PGV, and 5% Damped Linear Acceleration Response Spectra. *Earthquake Spectra*, *30*(3), 1087-1115. https://doi.org/10.1193/062913eqs175m

Chiou, B. S. J., & Youngs, R. R. (2014). Update of the Chiou and Youngs NGA Model for the Average Horizontal Component of Peak Ground Motion and Response Spectra. *Earthquake Spectra*, *30*(3), 1117-1153. https://doi.org/10.1193/072813eqs219m

Dibblee, T. W., & Minch, J. A. (2008). *Geologic map of the Lancaster & Alpine Butte 15 minute quadrangles, Los Angeles County, California*. Dibblee Geological Foundation.

Field, E. H., Biasi, G. P., Bird, P., Dawson, T. E., Felzer, K. R., David D. Jackson, Johnson, K. M., Jordan, T. H., Madden, C., Michael, A. J., Milner, K. R., Page, M. T., Parsons, T., Powers, P. M., Shaw, B. E., Thatcher, W. R., Ray J. Weldon, I., & Zeng, Y. (2013). *Uniform California earthquake rupture forecast, version 3 (UCERF3)—The time-independent model* (U.S. Geological Survey Open-File Report 2013–1165). http://pubs.usgs.gov/of/2013/1165/

Fumal, T. E., Weldon, R. J., II, Biasi, G. P., Dawson, T. E., Seitz, G. G., Frost, W. T., & Schwartz, D. P. (2002). Evidence for Large Earthquakes on the San Andreas Fault at the Wrightwood, California, Paleoseismic Site: a.d. 500 to Present. *Bulletin of the Seismological Society of America*, *92*(7), 2726-2760. https://doi.org/10.1785/0120000608

GeoPentech. (2015). *Southwestern United States Ground Motion Characterization SSHAC Level 3 – Technical Report Rev.2*. http://www.lettisci.com/sshac3/SWUS_GMC_TR_Main_Report.zip

Gerstenberger, M. C., Marzocchi, W., Allen, T., Pagani, M., Adams, J., Danciu, L., Field, E. H., Fujiwara, H., Luco, N., Ma, K. F., Meletti, C., & Petersen, M. D. (2020). Probabilistic Seismic Hazard Analysis at Regional and National Scales: State of the Art and Future Challenges. *Reviews of Geophysics*, *58*(2). https://doi.org/10.1029/2019rg000653

Grant Ludwig, L., Brune, J. N., Anooshehpoor, A., Purvance, M. D., Brune, R. J., & Lozos, J. C. (2015). Reconciling Precariously Balanced Rocks (PBRs) with Large Earthquakes on the San Andreas Fault System. *Seismological Research Letters*, *86*(5), 1345-1353. https://doi.org/10.1785/0220140239

Hall, C. M., Webb, H. N., Girty, G. H., Allam, A. A., & Rockwell, T. K. (2019). A case study of a precariously balanced rock, its partially exhumed corestone platform, and encasing saprock and soil. *Catena*, *172*, 719-737. https://doi.org/10.1016/j.catena.2018.09.029

Hanks, T. C., Abrahamson, N. A., Baker, J. W., Boore, D. M., Board, M., Brune, J. N., Cornell, C. A., & Whitney, J. W. (2013). *Extreme ground motions and Yucca Mountain*. https://pubs.er.usgs.gov/publication/ofr20131245

Hanks, T. C., Abrahamson, N. A., Boore, D. M., Coppersmith, K. J., & Knepprath, N. E. (2019). *Implementation of the SSHAC Guidelines for Level 3 and 4 PSHAs--experience gained from actual applications* (U.S. Geological Survey Open-File Report 2009-1093, Issue. http://pubs.usgs.gov/of/2009/1093/

Jayaram, N., & Baker, J. W. (2009). Correlation model for spatially distributed ground-motion intensities. *Earthquake Engineering & Structural Dynamics*, *38*(15), 1687-1708. https://doi.org/10.1002/eqe.922

Kulkarni, R. B., Youngs, R. R., & Coppersmith, K. J. (1984). Assessment of confidence intervals for results of seismic hazard analysis. Proceedings of 8th World Conference on Earthquake Engineering, San Francisco, CA.

Lozos, J. C., Olsen, K. B., Brune, J. N., Takedatsu, R., Brune, R. J., & Oglesby, D. D. (2015). Broadband Ground Motions from Dynamic Models of Rupture on the Northern San Jacinto Fault, and Comparison with Precariously Balanced Rocks. *Bulletin of the Seismological Society of America*, *105*(4), 1947-1960. https://doi.org/10.1785/0120140328

Oberlander, T. M. (1972). Morphogenesis of Granitic Boulder Slopes in the Mojave Desert, California. *The Journal of Geology*, *80*(1), 1-20.

Olsen, K., & Brune, J. (2008). Constraints from precariously balanced rocks on preferred rupture directions for large earthquakes on the southern San Andreas Fault. *Journal of Seismology*, *12*, 235-241. https://doi.org/10.1007/s10950-007-9078-7

Page, M. T., Field, E. H., Milner, K. R., & Powers, P. M. (2014). The UCERF3 Grand Inversion: Solving for the Long-Term Rate of Ruptures in a Fault System. *Bulletin of the Seismological Society of America*, *104*(3), 1181-1204. https://doi.org/10.1785/0120130180

Purvance, M. D., Anooshehpoor, A., & Brune, J. (2008a). Freestanding block overturning fragilities: Numerical simulation and experimental validation. *Earthquake Engineering & Structural Dynamics*, *37*(5), 791-808. https://doi.org/10.1002/eqe.789

Purvance, M. D., Brune, J. N., Abrahamson, N. A., & Anderson, J. G. (2008b). Consistency of Precariously Balanced Rocks with Probabilistic Seismic Hazard Estimates in Southern California. *Bulletin of the Seismological Society of America*, *98*(6), 2629-2640. https://doi.org/10.1785/0120080169

Rodriguez-Marek, A., Rathje, E. M., Bommer, J. J., Scherbaum, F., & Stafford, P. J. (2014). Application of Single-Station Sigma and Site-Response Characterization in a Probabilistic Seismic-Hazard Analysis for a New Nuclear Site. *Bulletin of the Seismological Society of America*, *104*(4), 1601-1619. https://doi.org/10.1785/0120130196

Rood, A. H., Rood, D. H., Balco, G., Stafford, P. J., Ludwig, L. G., Kendrick, K. J., & Wilcken, K. M. (*2022*). Validation of earthquake ground-motion models in southern California, USA, using precariously balanced rocks. *GSA Bulletin*. https://doi.org/10.1130/b36484.1

Rood, A. H., Rood, D. H., Stirling, M. W., Madugo, C. M., Abrahamson, N. A., Wilcken, K. M., Gonzalez, T., Kottke, A., Whittaker, A. C., Page, W. D., & Stafford, P. J. (2020). Earthquake Hazard Uncertainties Improved Using Precariously Balanced Rocks. *AGU Advances*, *1*(4). https://doi.org/10.1029/2020av000182

Scharer, K. M., Weldon, R. J., II, Fumal, T. E., & Biasi, G. P. (2007). Paleoearthquakes on the Southern San Andreas Fault, Wrightwood, California, 3000 to 1500 b.c.: A New Method for Evaluating Paleoseismic Evidence and Earthquake Horizons. *Bulletin of the Seismological Society of America*, *97*(4), 1054-1093. https://doi.org/10.1785/0120060137

Sieh, K., Stuiver, M., & Brillinger, D. (1989). A more precise chronology of earthquakes produced by the San Andreas Fault in southern California. *Journal of Geophysical Research*, *94*(B1). https://doi.org/10.1029/JB094iB01p00603

SSHAC (Senior Seismic Hazard Analysis Committee). (1997). *Recommendations for Probabilistic Seismic Hazard Analysis: Guidance on Uncertainty and Use of Experts*. https://www.nrc.gov/docs/ML0800/ML080090003.pdf

SSHAC (Senior Seismic Hazard Analysis Committee). (2012). *Practical Implementation Guidelines for SSHAC Level 3 and 4 Hazard Studies*. U. S. N. R. Commission. https://www.nrc.gov/docs/ML1211/ML12118A445.pdf

Stafford, P. J. (2012). Evaluation of structural performance in the immediate aftermath of an earthquake: a case study of the 2011 Christchurch earthquake. *International Journal of Forensic Engineering*, *1*(1), 58-77.

Stirling, M. W., Abbott, E. R., Rood, D. H., McVerry, G. H., Abrahamson, N. A., Barrell, D. J. A., Huso, R., Litchfield, N. J., Luna, L., Rhoades, D. A., Silvester, P., Van Dissen, R. J., Van Houtte, C., & Zondervan, A. (2021). First Use of Fragile Geologic Features to Set the Design Motions for a Major Existing Engineered Structure. *Bulletin of the Seismological Society of America*. https://doi.org/10.1785/0120210026

Stirling, M. W., Anooshehpoor, A., Brune, J. N., Biasi, G. P., & Wesnousky, S. G. (2002). Assessment of the Site Conditions of Precariously Balanced Rocks in the Mojave Desert, Southern California. *Bulletin of the Seismological Society of America*, *92*(6), 2139–2214. https://doi.org/10.1785/0120010221

Stirling, M. W., Oskin, M. E., Arrowsmith, J. R., Rood, A. H., Goulet, C. A., Grant Ludwig, L., King, T. R., Kottke, A., Lozos, J. C., Madugo, C. M., McPhillips, D., Rood, D. H., Sleep, N. H., & Wittich, C. E. (2020). Evaluation of Seismic Hazard Models with Fragile Geologic Features. *Seismological Research Letters*, *92 (1)*, 314-324. 10.1785/0220200197

Thompson, E. M., Wald, D. J., & Worden, C. B. (2014). A VS30 Map for California with Geologic and Topographic Constraints. *Bulletin of the Seismological Society of America*, *104*(5), 2313-2321. https://doi.org/10.1785/0120130312

Toppozada, T. R., Branum, D. M., Reichle, M. S., & Hallstrom, C. L. (2002). San Andreas Fault Zone, California: M ≥5.5 Earthquake History. *Bulletin of the Seismological Society of America*, *92*(7), 2555-2601. https://doi.org/10.1785/0120000614

Veeraraghavan, S., Heaton, T. H., & Krishnan, S. (2019). Lower Bounds on Ground Motion at Point Reyes during the 1906 San Francisco Earthquake from Train Toppling Analysis. *Seismological Research Letters*, *90*(2A), 683-691. https://doi.org/10.1785/0220180327

Wald, D. J., Quitoriano, V., Heaton, T. H., & Kanamori, H. (1999). Relationships between Peak Ground Acceleration, Peak Ground Velocity, and Modified Mercalli Intensity in California. *Earthquake Spectra*, *15*(3), 557-564. https://doi.org/10.1193/1.1586058

Weldon, R., Scharer, K., Fumal, T., & Biasi, G. (2004). Wrightwood and the earthquake cycle: What a long recurrence record tells us about how faults work. *GSA Today*, *14*(9), 4-10. https://doi.org/10.1130/1052-5173(2004)014<4:WATECW>2.0.CO;2

Zielke, O., Arrowsmith, J. R., Grant Ludwig, L., & Akciz, S. O. (2012). High-Resolution Topography-Derived Offsets along the 1857 Fort Tejon Earthquake Rupture Trace, San Andreas Fault. *Bulletin of the Seismological Society of America*, *102*(3), 1135-1154. https://doi.org/10.1785/0120110230

AUTHOR MAILING ADDRESSES

Anna Rood: Global Earthquake Model (GEM) Foundation, 27100 Pavia, Italy.

Anna Rood: Department of Civil and Environmental Engineering, Imperial College London, London, SW7 2AZ, UK.

Peter Stafford: Department of Civil and Environmental Engineering, Imperial College London, London, SW7 2AZ, UK.

Dylan Rood: Department of Earth Science and Engineering, Imperial College London, London, SW7 2AZ, UK.

854 TABLE 1. Lovejoy Buttes PBR data

PBR	Geometric Parameters*				Fragility Function (g) *†			Fragility Age (ka)*			Weighted mean probability of survival §
	α_1	α_2	R_1	R_2	Percentile			Percentile			
	(rad)	(rad)	(m)	(m)	25	50	75	16	50	84	
LB05	0.34	0.47	0.49	0.42	0.88	1.01	1.12	10.3	28.5	30.9	0.15
LJ1	0.31	0.48	1.90	1.55	1.34	1.65	1.87	9.5	9.9	10.4	0.41
LJ5	0.42	0.44	0.87	0.81	1.44	1.69	1.84	48.3	49.9	51.1	0.25
LJB1	0.21	0.42	0.95	0.92	0.55	0.66	0.73	9.4	10.5	11.8	0.04
LJB2	0.16	0.60	0.46	0.42	0.60	0.69	0.76	7.9	14.0	19.5	0.05

* From Rood *et al.* (*2022*).
† Median fragility function calculated using the equations of Purvance *et al.* (2008a). α_2 values of greater than 0.5 radians were set to 0.5 radians in the equations of Purvance *et al.* (2008a).
§ Probability of survival of the PBR over its fragility age to the present day calculated for each of the 207 hazard curves weighted by the end-branch weight of the hazard curve.

855

LIST OF FIGURE CAPTIONS

Figure 1. (a) Regional map of southern California. Red lines are the surface traces of faults used in the UCERF3 seismic source characterization for California (Field *et al.*, 2013). The San Andreas fault is labeled and the Mojave South section is the bold yellow line. The 1812 Wrightwood rupture is shown in the black dashed line (Toppozada *et al.*, 2002) and the 1857 Fort Tejon rupture is shown in the blue dashed line (Fumal *et al.*, 2002; Weldon *et al.*, 2004). The black box shows the location of panel B. (b) Map of the Mojave South section of the San Andreas fault around the - Lovejoy Buttes site. Blue circles are the NGA-West2 recording stations (Ancheta *et al.*, 2014) used to estimate the site term at the Lovejoy Buttes site. Stations are labeled in white with their NGA-West stations names. Black triangles, labelled in black, are paleoseismic trench sites used in UCERF3. The hillshade was calculated from the 1m USGS 3DEP lidar dataset sourced from OpenTopography.org. The white box shows the location of Figure 1c. (c) Map of Lovejoy Buttes. Yellow triangles show the location of the five PBRs at the Lovejoy Buttes site. PBRs with the prefix LJB are located in a different drainage catchment from PBRs with the prefix LJ, which is also in a different drainage catchment from PBRs with the prefix LB.

Figure 2. *Ground-motion characterization (GMC) logic tree for the Lovejoy Buttes site. The parameter modeled in each node is labeled in each header. The weight of each sub-branch is in blue brackets. The base models shown are the DCPP common-form models that have a non-zero weight (see Table A2). Each base model is the representative model selected for every discretized cell of the 2-D Sammon's map representation. The 23 base model branches, three site term branches, and three sigma branches result in 207 realizations through our GMC model logic tree. Each path through the logic tree has an end-branch weight that corresponds to the product of the weights from each of the three nodes. For example, Model 1, with a high site term, and high sigma has an end-branch weight of (0.151 x 0.2 x 0.3) 0.00906.*

Figure 3. *Lovejoy Buttes site term analysis. (A) Blue circles are empirical semivariograms calculated for each of the NGA-West2 ground-motion models. Black lines are the fitted exponential semivariogram for each ground-motion model. (B) Station-residual of the NGA-West2 recording stations within 30 km of Lovejoy Buttes, which were used to make the conditional prediction of the site term at Lovejoy Buttes. The size and color of the circles correspond to the site term at each of these stations.*

Figure 4. *Fragility functions calculated for the five Lovejoy Buttes precariously balanced rocks (PBRs). The dotted line is the most fragile fragility level and the dashed line is the least fragile fragility level.*

Figure 5. *Hazard curves calculated for the Lovejoy Buttes site. Light gray curves are the individual 207 hazard curve estimates output from our PSHA model. The original mean curve (yellow line), median estimate (bold black line), 16^{th} – 84^{th} fractile uncertainty (solid black lines) and 5^{th} – 95^{th} fractile uncertainty (dashed black lines) are shown. The mean curve (green line), median estimate (bold blue line), 16^{th} – 84^{th} fractile uncertainty (solid blue lines) and 5^{th} – 95^{th} fractile uncertainty (dashed blue lines) after the end branch reweighting are shown.*

APPENDICIES

Table A1. San Andreas fault Mojave South rupture rates.

Magnitude (Mw)	Participation Rate (yr^{-1})		
	Weighted Mean	Maximum	Minimum
5.05	0.00E+00	0.00E+00	0.00E+00
5.15	0.00E+00	0.00E+00	0.00E+00
5.25	0.00E+00	0.00E+00	0.00E+00
5.35	0.00E+00	0.00E+00	0.00E+00
5.45	0.00E+00	0.00E+00	0.00E+00
5.55	0.00E+00	0.00E+00	0.00E+00
5.65	0.00E+00	0.00E+00	0.00E+00
5.75	0.00E+00	0.00E+00	0.00E+00
5.85	0.00E+00	0.00E+00	0.00E+00
5.95	0.00E+00	0.00E+00	0.00E+00
6.05	0.00E+00	0.00E+00	0.00E+00
6.15	0.00E+00	0.00E+00	0.00E+00
6.25	1.30E-03	9.20E-03	0.00E+00
6.35	1.02E-03	8.39E-03	0.00E+00
6.45	6.34E-03	1.72E-02	3.86E-04
6.55	8.24E-04	8.19E-03	0.00E+00
6.65	8.69E-05	5.77E-04	3.39E-05
6.75	1.16E-04	5.50E-04	3.80E-05
6.85	1.27E-04	4.04E-04	3.82E-05
6.95	1.10E-04	2.89E-04	3.08E-05
7.05	1.08E-04	1.94E-04	7.07E-06
7.15	1.76E-04	4.95E-04	3.03E-06
7.25	2.55E-04	1.47E-03	2.70E-06
7.35	6.18E-05	1.27E-03	2.49E-06
7.45	9.44E-05	1.13E-03	3.03E-06
7.55	5.51E-05	7.99E-04	3.45E-06
7.65	9.01E-05	7.25E-04	5.37E-06
7.75	3.77E-04	1.69E-03	1.57E-05
7.85	1.07E-03	1.56E-03	4.96E-04
7.95	9.88E-04	1.34E-03	3.31E-04
8.05	8.02E-04	1.23E-03	3.11E-05
8.15	5.96E-04	1.28E-03	1.41E-05
8.25	3.68E-04	1.02E-03	7.17E-07
8.35	3.48E-05	6.68E-04	0.00E+00
8.45	3.05E-06	3.52E-04	0.00E+00
8.55	1.61E-06	4.06E-05	0.00E+00
8.65	0.00E+00	0.00E+00	0.00E+00
8.75	0.00E+00	0.00E+00	0.00E+00
8.85	0.00E+00	0.00E+00	0.00E+00
8.95	0.00E+00	0.00E+00	0.00E+00
9.05	0.00E+00	0.00E+00	0.00E+00

Notes: See Data and Resources section for data accessibility.

898 Table A2. DCPP common-form model coefficients.

Model ID	a0	a1	a2	a3	a4	a5	a6	a7	a8	a10	Weight
Model 1	0.947835	0.235435	0.959904	-0.097895	-1.199400	0.182303	5.825900	0.094325	0.150917	0.286206	0.150923
Model 2	0.000000	0.000000	0.000000	0.000000	0.000000	0.000000	0.000000	0.000000	0.000000	0.000000	0.000000
Model 3	0.743320	0.211259	0.399652	-0.317621	-1.195390	0.280279	5.088230	0.112296	0.195828	0.225597	0.085294
Model 4	0.000000	0.000000	0.000000	0.000000	0.000000	0.000000	0.000000	0.000000	0.000000	0.000000	0.000000
Model 5	1.107110	0.113193	0.820097	-0.144622	-1.296210	0.225163	6.161460	0.062386	-0.063002	0.160493	0.055704
Model 6	0.909303	0.055758	0.805807	-0.213959	-1.271470	0.229798	5.402060	0.108269	0.149545	0.297034	0.055210
Model 7	0.113017	0.174711	0.254003	-0.025578	-0.915986	0.188868	3.742940	0.134445	0.096891	0.316098	0.084428
Model 8	0.000000	0.000000	0.000000	0.000000	0.000000	0.000000	0.000000	0.000000	0.000000	0.000000	0.000000
Model 9	0.000000	0.000000	0.000000	0.000000	0.000000	0.000000	0.000000	0.000000	0.000000	0.000000	0.000000
Model 10	0.000000	0.000000	0.000000	0.000000	0.000000	0.000000	0.000000	0.000000	0.000000	0.000000	0.000000
Model 11	0.000000	0.000000	0.000000	0.000000	0.000000	0.000000	0.000000	0.000000	0.000000	0.000000	0.000000
Model 12	0.866509	-0.230442	0.293812	-0.514397	-1.506010	0.405356	4.767530	0.070935	0.282461	-0.108877	0.021663
Model 13	0.672015	0.038727	0.908551	-0.177023	-1.117950	0.217171	4.404030	0.088372	0.167082	0.365773	0.031211
Model 14	1.476020	-0.217563	0.750171	-0.434190	-1.632370	0.336537	6.326790	0.063385	0.238831	0.139699	0.014687
Model 15	1.071830	-0.184811	0.292423	-0.488303	-1.591260	0.391309	5.427050	0.085901	0.253045	0.169363	0.046233
Model 16	0.257188	-0.016407	0.456890	-0.207547	-1.149890	0.289765	3.682790	0.075863	0.156210	0.179612	0.021812
Model 17	1.582910	-0.089125	0.769286	-0.312390	-1.667280	0.307501	6.888470	0.040689	0.042678	0.096641	0.079709
Model 18	0.716620	0.043841	0.604941	-0.145364	-1.288000	0.239233	5.602400	0.041602	0.109157	0.168608	0.037345
Model 19	0.000000	0.000000	0.000000	0.000000	0.000000	0.000000	0.000000	0.000000	0.000000	0.000000	0.000000
Model 20	-0.568032	0.438637	1.305150	0.111746	-0.534038	0.156661	2.636000	0.169645	0.137226	0.297492	0.053547
Model 21	0.000000	0.000000	0.000000	0.000000	0.000000	0.000000	0.000000	0.000000	0.000000	0.000000	0.000000
Model 22	1.495530	-0.245945	0.428190	-0.518509	-1.724040	0.383693	6.132830	-0.010406	0.325181	0.073241	0.020270
Model 23	2.471880	-0.333467	-0.218869	-0.696142	-2.063600	0.376886	8.376130	-0.038492	0.297369	0.006180	0.014286
Model 24	0.214452	0.068324	1.332880	-0.223712	-0.968908	0.269785	3.665250	0.171340	0.281014	-0.033868	0.024008

Model 25	0.108244	0.291060	0.800682	0.235796	-0.757364	0.104589	4.241460	0.108305	-0.151399	0.473280	0.012571
Model 26	0.637536	-0.057509	1.209500	-0.303396	-1.237150	0.260041	4.353810	0.127726	0.218253	0.223205	0.024430
Model 27	0.858958	0.197780	0.342436	0.090260	-1.158250	0.123513	6.429500	0.028896	-0.002465	0.403333	0.011278
Model 28	1.037870	0.245207	0.553755	0.021423	-1.227930	0.102204	6.692870	0.023625	0.052078	0.228292	0.043343
Model 29	1.893430	0.188045	0.334012	-0.266295	-1.650480	0.165120	7.467130	0.051503	0.114941	0.421662	0.067510
Model 30	0.719697	0.128966	0.163630	-0.050983	-1.259890	0.150276	5.547270	0.034050	0.081649	-0.035145	0.018987
Model 31	1.163200	-0.225873	0.347216	-0.375644	-1.604540	0.229903	5.754700	0.016949	0.117533	0.065275	0.025552

Notes:

Nine of the 31 DCPP common-form models have coefficients of zero and a weight of zero, so do not produce a hazard estimate. Therefore, these nine models were not included in the GMC model, which leaves 23 models that were used (Figure 2).

See Data and Resources section for data accessibility.

900 Table A3. Empirical semivariogram for each of the four NGA-West2 GMMs.

901

NGA-West GMM	a (range)	b (sill)	C_0 (nugget)
ASK14	36.2683	0.0599	0.0900
BSSA14	23.3046	0.0523	0.0714
CB14	29.0604	0.0512	0.0706
CY14	26.1758	0.0489	0.0689

Figure 1

Click here to access/download;Figure;Site_specific_map_ruptures.png

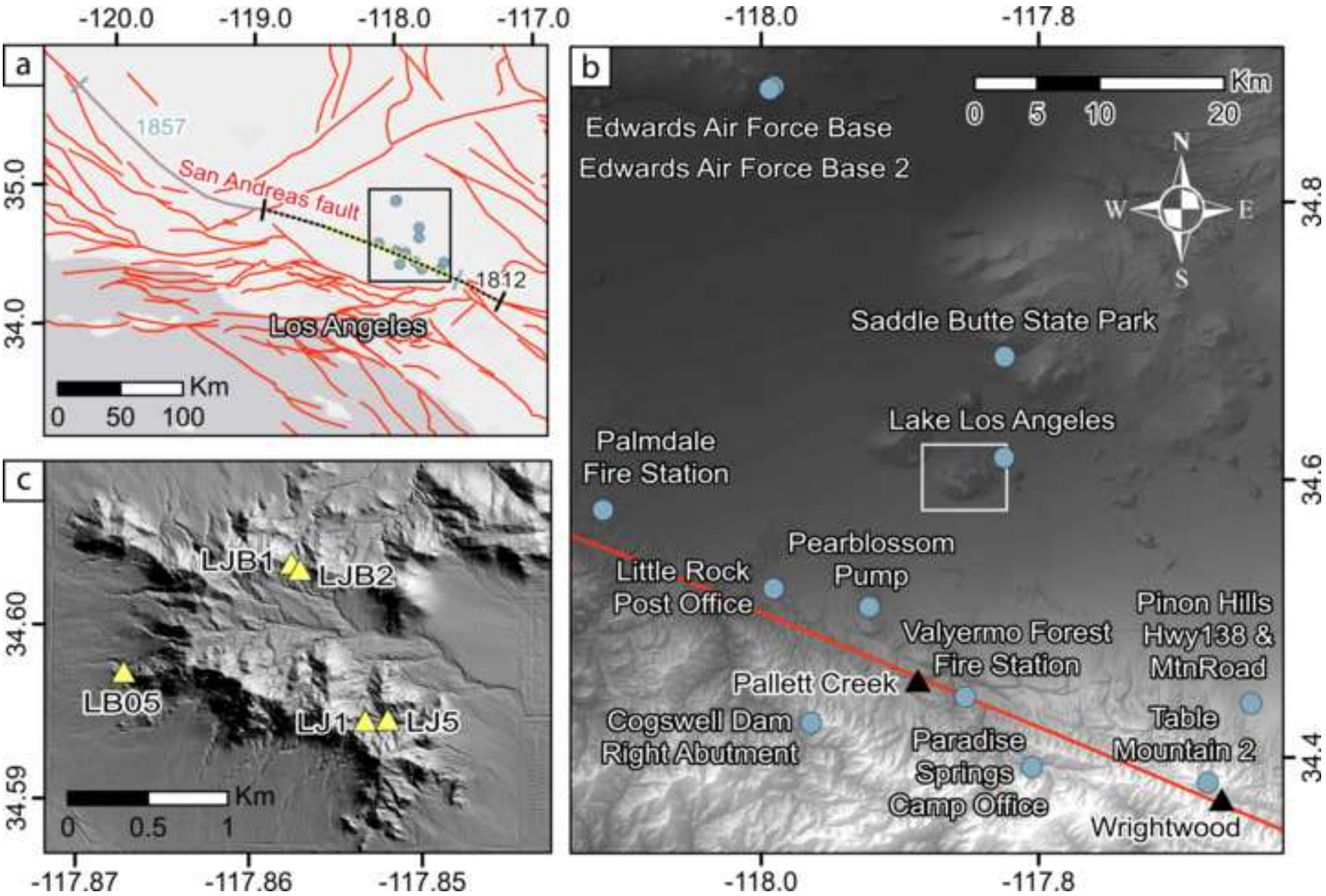


Figure 2

Click here to access/download;Figure;Logic_tree.ai.png

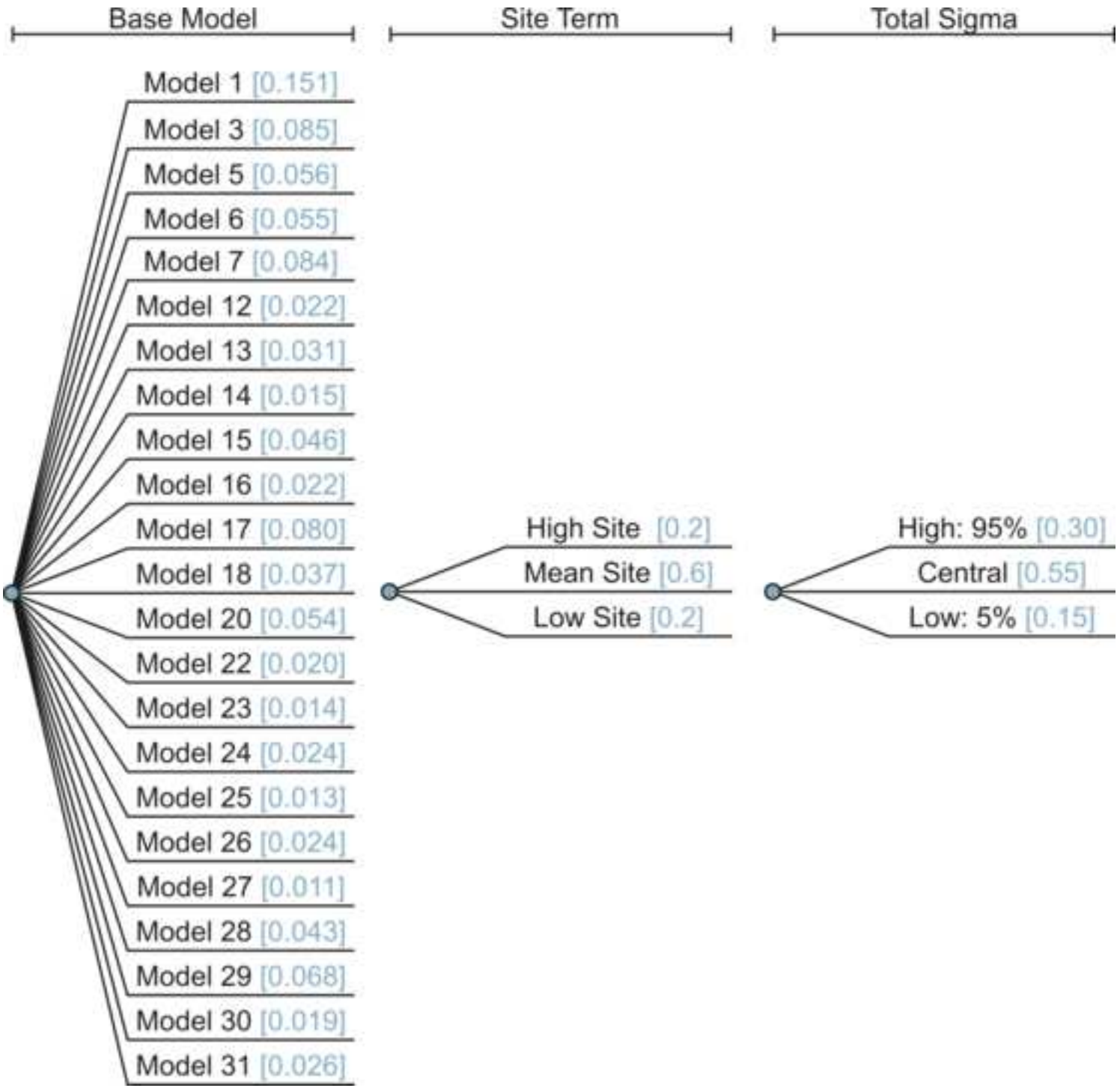


Figure 3

Click here to access/download;Figure;Site_term_figure.png

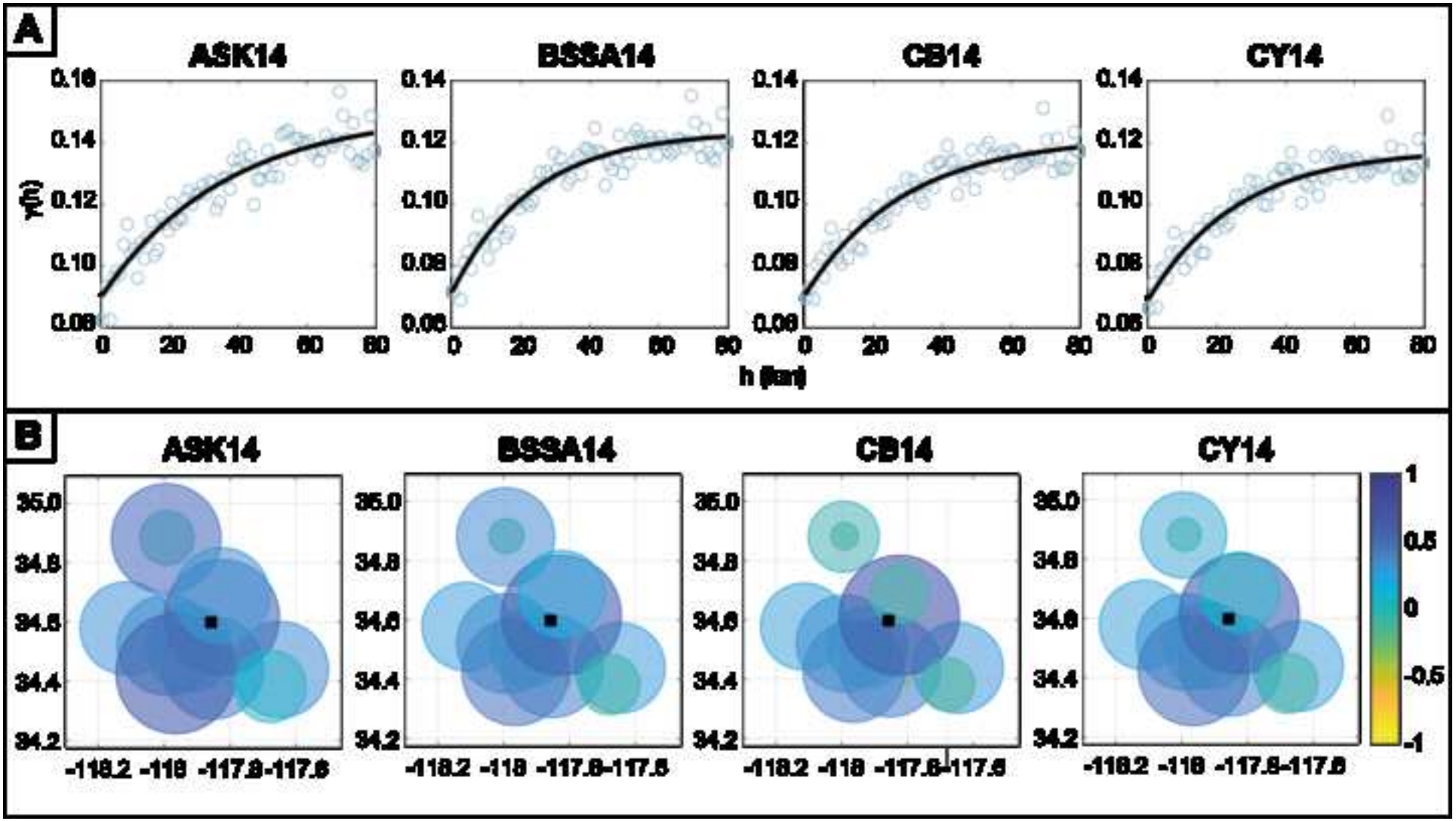
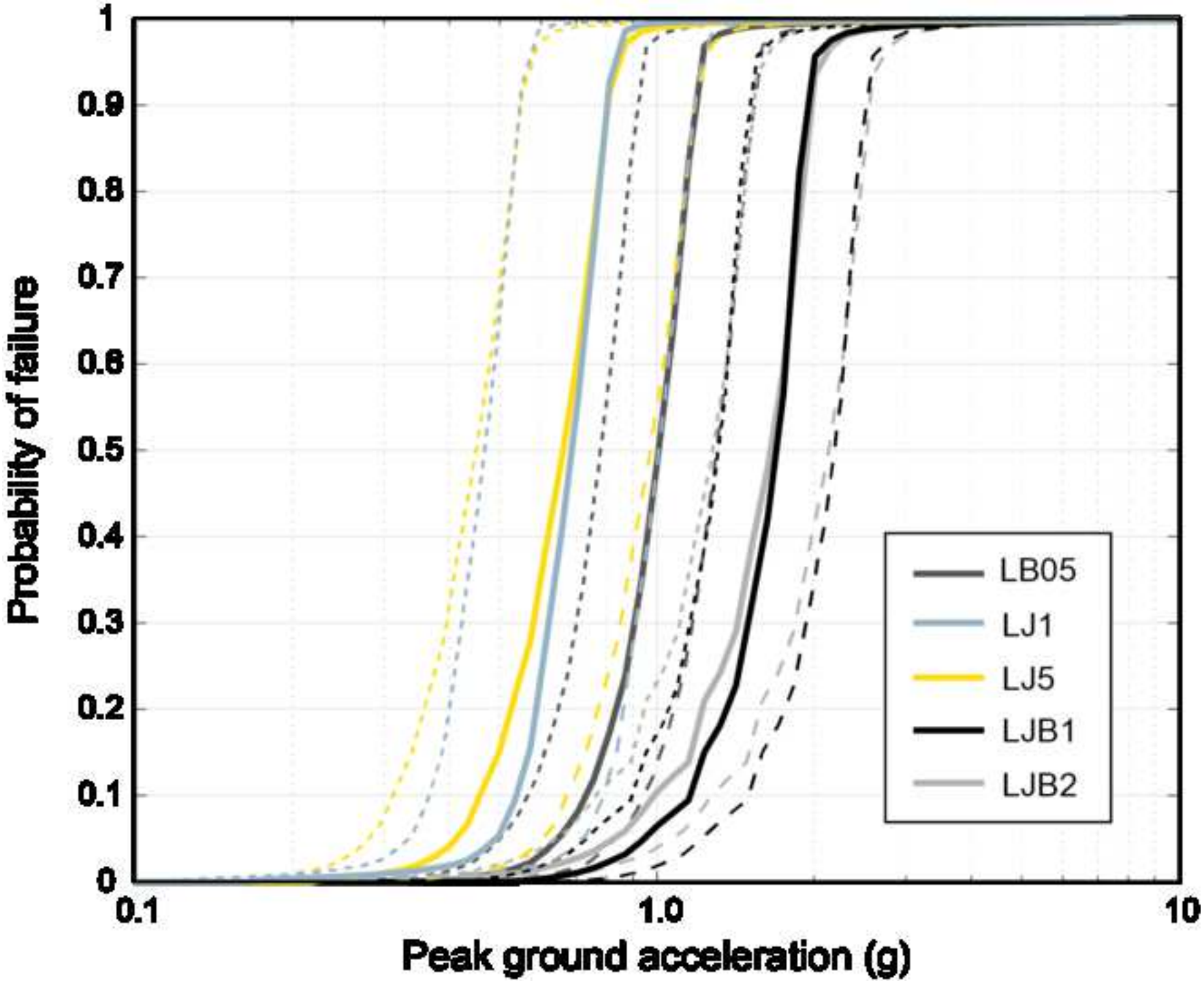


Figure 4

Click here to access/download;Figure;Fragility_function_figure.png



Figure

Click here to access/download;Figure;Old_new_curves_percentiles.ai.png

